PHYSICAL REVIEW B **90**, 020509(R) (2014)

Honeycomb, square, and kagome vortex lattices in superconducting systems with multiscale intervortex interactions

Qingyou Meng,[1] Christopher N. Varney,[2] Hans Fangohr,[3] and Egor Babaev[4,1]
[1]*Department of Physics, University of Massachusetts, Amherst, Massachusetts 01003, USA*
[2]*Department of Physics, University of West Florida, Pensacola, Florida 32514, USA*
[3]*Engineering and the Environment, University of Southampton, Southampton SO17 1BJ, United Kingdom*
[4]*Department of Theoretical Physics, The Royal Institute of Technology, SE-10691 Stockholm, Sweden*
(Received 16 April 2014; revised manuscript received 9 July 2014; published 29 July 2014)

The recent proposal of Romero-Isart *et al.* [Phys. Rev. Lett. **111**, 145304 (2013)] to utilize the vortex lattice phases of superconducting materials to prepare a lattice for ultracold-atom-based quantum emulators raises the need to create and control vortex lattices of different symmetries. Here we propose a mechanism by which honeycomb, hexagonal, square, and kagome vortex lattices could be created in superconducting systems with multiscale intervortex interactions. Multiple scales of the intervortex interaction can be created and controlled in layered systems made of different superconducting materials or with differing interlayer spacings.

DOI: 10.1103/PhysRevB.90.020509 PACS number(s): 67.85.−d, 74.25.Uv

To circumvent the limitations on classical computation, a growing effort to manipulate and control the behavior of ultracold atomic gases has led to these systems being used as quantum simulators for a host of phenomena in condensed matter physics [1,2]. A focus of quantum simulator investigations has been on building Hubbard models by loading a gas of neutral atoms into optical lattices and tuning the interaction between the atoms [3,4]. At present, great strides have been made in cooling protocols [5–7], but the main question, to assess in such experiments whether the Hubbard model can explain high-T_c superconductivity, remains unanswered.

In order to address this question, better cooling schemes which reduce the entropy of the quantum simulator are necessary [4]. Very recently, Romero-Isart *et al.* [8] proposed placing ultracold atoms in a lattice potential generated by a magnetic field of superconducting vortices in type-2 superconductors and trapping the atoms near the surface. This new approach aims to decrease the interlattice site distance, making the required regimes experimentally feasible [8,9]. This possibility of a crucially important application raises the need to create and control vortex lattices of different symmetries. Although in some exotic cases a square vortex lattice has been observed [10,11], the overwhelming majority of vortex lattices in superconductors have hexagonal symmetry. In order to create a vortex lattice of various symmetries for quantum emulators, Romero-Isart *et al.* [8] proposed pinning the vortices in arrays of etched holes or antidots [12]. While such vortex systems have been extensively investigated in superconductivity both theoretically and experimentally for various pinning array geometries [13–22], Romero-Isart *et al.* [8] note that the anticipated challenges to implementing the approach are high requirements for perfection of the vortex lattice and possible variations and field inhomogeneities in the antidot arrays. In fact, the interest in self-assembly of kagome and honeycomb structures goes beyond the recent interest in vortex matter and is intensively studied in soft condensed matter systems [23–26].

Here we propose an alternative approach involving multicomponent superconducting systems. Recently there has been interest in superconductivity with several scales of repulsive and attractive interaction. In two-band superconductors it is possible to have a vortex system where the short-range interactions are repulsive while the long-range interactions are attractive in regimes where one coherence length is shorter than the magnetic field penetration length while the second coherence length is larger, i.e., $\xi_1 < \lambda < \xi_2$ [27–30]. The regime was recently termed type-1.5 superconductivity in experimental works on MgB_2 [31–33] and Sr_2RuO_4 [34,35]. The nonmonotonic intervortex interaction is also possible in electromagnetically or proximity-effect coupled bilayers [27].

In the two-band superconductor the long-range intervortex interaction energy is given by [27,28,36]

$$E_{\rm int} = C_B^2 K_0\left(\frac{r}{\lambda}\right) - C_1^2 2\pi K_0\left(\frac{r}{\xi_1}\right) - C_2^2 K_0\left(\frac{r}{\xi_2}\right). \quad (1)$$

The first term describes intervortex repulsion which comes from magnetic and current-current interaction. The second and third terms describe attractive interactions from core overlaps. The two contributions are due to to coherence lengths.

In Ref. [37] it was proposed that in layered systems multiple repulsive length scales are possible when different layers have different λ_i. For a straight and rigid vortex line, the long-range interaction is then

$$E_{\rm int} = \sum_i C_{B_i}^2 K_0\left(\frac{r}{\lambda_i}\right) - \sum_j C_j^2 2\pi K_0\left(\frac{r}{\xi_j}\right). \quad (2)$$

Such a system can have various cluster phases due to multiscale repulsive interactions [37]. Subsequently some of the phases obtained in simulations where the vortices are treated as a point particle [37] were also obtained in simulations of a layered Ginzburg-Landau model [38].

Here we point out that layered systems proposed in Ref. [37], i.e., structures made of a combination of type-1 and type-2 superconductors with variable interlayer distances (see Fig. 1), could be used to create vortex lattice of different symmetries. In what follows, we utilize Langevin dynamics to study various states of vortex matter in superconductors [39–42]. Often in systems with multiple repulsive length scales, various phases are quite robust with respect to potential changes as long as the potential preserves the distinct repulsive length scales [43,44]. Thus we use a phenomenological

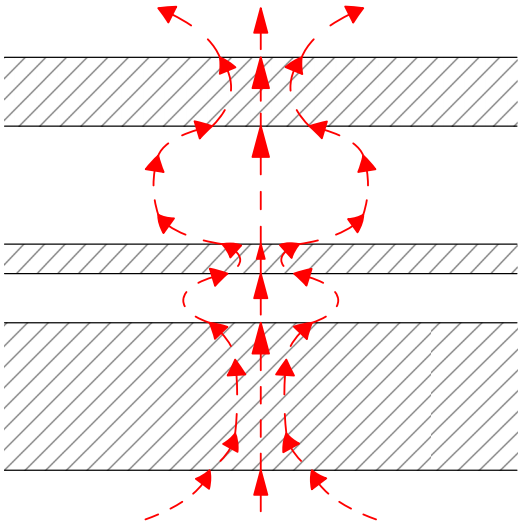

FIG. 1. (Color online) Schematic picture of the magnetic field lines of a vortex in a layered superconductor. Shaded (white) areas are superconductor (insulator) layers with different thicknesses. The flux spreads in the nonsuperconducting regions.

pairwise potential with multiple length scales which has characteristic features of the analytically known asymptotic form Eq. (2) as well as the included effect of a demagnetization field in the form of an analytically known long-range power-law repulsive intervortex force [45]. We demonstrate that layered systems where such a potential can be realized can be used to generate the four two-dimensional lattices: hexagonal, honeycomb, square, and kagome.

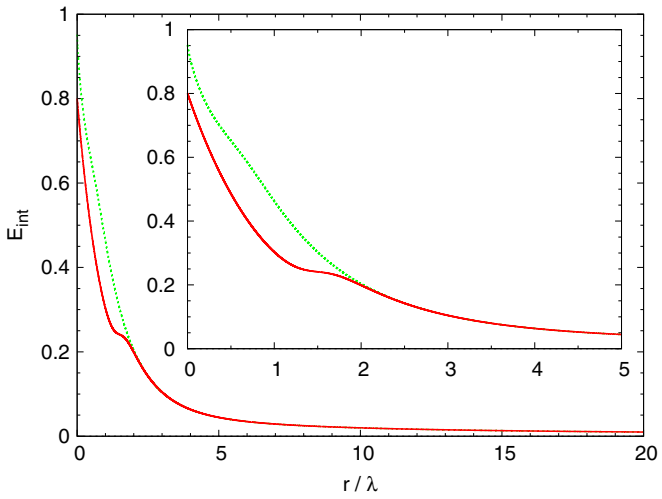

FIG. 2. (Color online) Phenomenological potential that describes the multiscale intervortex interaction for straight rigid vortex lines in a layered system with different layer parameters. The solid red curve gives rise to a honeycomb lattice at density [46] $\rho = 1.50$, a hexagonal lattice at $\rho = 2.25$, and a square lattice at $\rho = 2.50$, while for the dashed green line a kagome lattice is the ground state at a density of $\rho = 2.50$ [47].

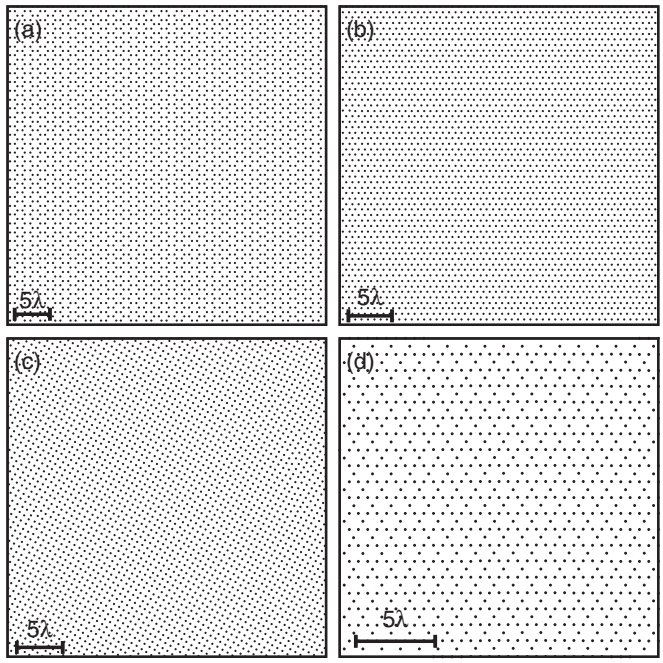

FIG. 3. The final vortex configuration at zero temperature for (a) $N_v = 3024$ and $\rho = 1.50$ (honeycomb lattice), (b) $N_v = 2958$ and $\rho = 2.25$ (hexagonal lattice), (c) $N_v = 2958$ and $\rho = 2.50$ (square lattice), and (d) $N_v = 1020$ and $\rho = 2.50$ (kagome lattice). (a)–(c) correspond to the solid red curve of Fig. 2, while (d) corresponds to the dashed green curve.

In Fig. 2, we illustrate two potentials that arise from a phenomenological form

$$E_{\rm int} = c_1 e^{-r/\lambda} - c_2 e^{-r/\xi} + c_3 \frac{\lambda\{\tanh[\alpha(r-\beta)]+1\}}{r+\delta} \quad (3)$$

that captures the essential multiscale features of the intervortex forces in a layered superconducting structure [37,47], when the interaction can be approximated by pairwise forces between straight vortex lines. The model features a short-range exponential repulsion, intermediate-ranged exponential attraction, and a long-range power-law repulsive behavior. The interplay between these different interactions results in a rich phase diagram which goes beyond the scope of this Rapid Communication; we defer a full discussion of its properties for future work [48].

In Fig. 3, we illustrate some of the ground state vortex phases of the potentials shown in Fig. 2. The phases were obtained using Langevin dynamics [40] simulations of $N_v \approx$ 1000–3000 vortices where the temperature was slowly reduced to $T = 0$ (see Refs. [37] and [48] for additional details). For the solid red line of Fig. 2, we obtain honeycomb, hexagonal, and square lattices at densities [46] $\rho = 1.50$, 2.25, and 2.50, respectively. For the dashed green curve, we obtain a perfect kagome lattice for $\rho = 2.50$. For the honeycomb, hexagonal, and square lattice results, we find little to no defects for the largest system sizes studied. For the kagome lattice results, we achieve a defect-free lattice for 1020 vortices but observe a kagome lattice with defects for 2958 vortices, which may be a consequence of the simulated annealing rate. All simulations were initialized with random configurations

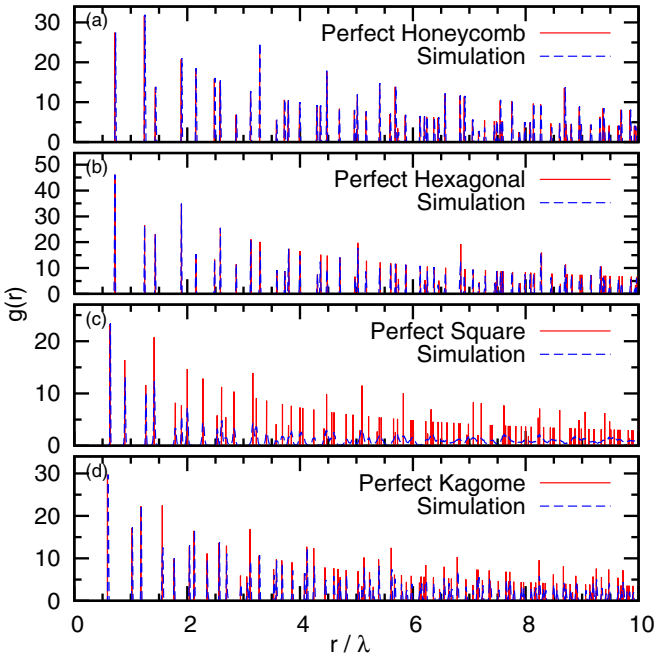

FIG. 4. (Color online) Comparison of the radial distribution function $g(r)$ of the vortex configurations shown in Fig. 3 with those of the ideal geometry for (a) honeycomb, (b) hexagonal, (c) square, and (d) kagome lattices. The dashed blue line is the zero temperature result after simulated annealing, and the solid red line is the ideal result.

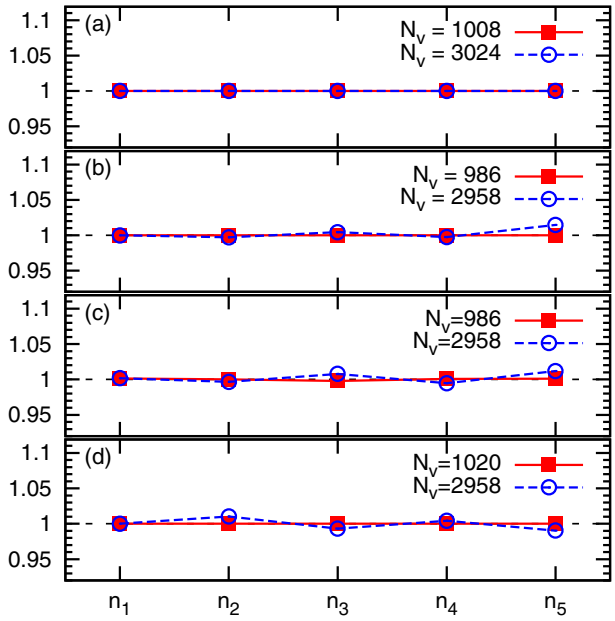

FIG. 5. (Color online) Number of nearest neighbors n_i up to the fifth nearest neighbor for the (a) honeycomb (b) hexagonal, (c) square, and (d) kagome lattices of Fig. 3 with $N_v \approx 1000$ (squares) and 3000 (circles) vortices. Here, n_i is normalized to the number of neighbors in a perfect lattice.

and later compared with a perfect lattice. In the case of the honeycomb and kagome lattice results, we observed a polycrystalline state which had higher energy than the perfect lattice. To ensure that the perfect lattice was the correct ground state, we prepared simulations with the ground state configuration at high temperature and repeated the simulated annealing protocol, ending up with a final configuration lower in energy than the defect-filled case (see Fig. 3(a) and 3(d) for lowest energy configurations).

In order to characterize the degree of perfection for each phase, we first consider the radial distribution function (RDF),

$$g(r) = \frac{1}{2\pi r \Delta r \rho N_v} \sum_{i=1}^{N_v} n_i(r, \Delta r), \tag{4}$$

where $n_i(r, \Delta r)$ is the number of particles in the shell surrounding the ith particle with radius r and thickness Δr. For phases that form regular lattice structures, we can offer a direct comparison with an ideal lattice, which we illustrate in Fig. 4.

From $g(r)$ we can define the ith nearest neighbor (coordination numbers) as

$$n_i = 2\pi\rho \int_{r_{i-1}}^{r_i} g(r) dr, \tag{5}$$

where r_{i-1} and r_i are the minima surrounding the ith peak in $g(r)$. In Fig. 5, we show the coordination number up to the fifth nearest neighbor for each of the lattices shown above.

Next, we define the degree of perfection $d = \frac{1}{N_v} \sum d_j$ for a lattice as

$$d_j = \frac{1}{n_1} \left| \sum_{i=1}^{n_1} \left(1 - \frac{\Delta\theta}{\theta_{\text{perfect}}} \right) \right|, \quad \Delta\theta = |\theta_i - \theta_{\text{perfect}}|, \tag{6}$$

where d_j is the degree of perfection for the jth vortex, n_1 is the number of the nearest neighbors (i.e., the number of the vortices within a circle of radius r_c with the jth vortex at its center, where r_c is the first minimum of the RDF), θ_i is the angle between the two nearest neighbors, and θ_{perfect} is the angle between the two nearest neighbors in the perfect lattice. Note that, by definition, $d = 1$ if there are no defects in the lattice. For the square, hexagonal, and honeycomb lattices $\theta_{\text{perfect}} = \pi/2, \pi/3$, and $2\pi/3$, respectively, while the kagome lattice has two possible angles, $\pi/3$ and $2\pi/3$.

For the honeycomb lattice [Figs. 3(a), 4(a), and 5(a)], we find that the ordering of the vortices matches the ideal result very well, with the degree of perfection $d \approx 1$ for all simulations of $N_v = 1008$ and 3024 vortices. The peaks of the radial distribution function closely match the ideal case, with broadening of the peaks due to defects that increases as the separation between the vortices increases. The coordination number is within 1% for all results.

For the hexagonal lattice [Figs. 3(b), 4(b), and 5(b)], the ordering is nearly perfect, with $d \approx 1$ and a radial distribution function featuring nearly delta function peaks that match with the ideal result. The coordination number calculation also remains within 1% of the ideal result up to n_5 for simulations of $N_v = 2958$ and for all coordination numbers we calculated for simulations of $N_v = 986$ vortices.

For the square lattice [Figs. 3(c), 4(c), and 5(c)], the ordering is extremely good, with $d = 0.990$ and 0.989 for

$N_v = 986$ and 2958 vortices, respectively. The radial distribution function features delta function peaks for the first eight peaks before broadening begins to occur. In addition, the number of nearest neighbors calculated is within 1% of the ideal result for the first five neighbors.

For the kagome lattice [Figs. 3(d), 4(d), and 5(d)], the ordering is also very good, with $d = 0.999$ and 0.946 for $N_v = 1020$ and 2958, respectively. The radial distribution function of the simulation result matches the perfect kagome lattice peaks very well. The coordination numbers are within 1% for both $N_v = 1020$ and 2958 vortices.

In summary, the recent proposal [8] of realizing quantum emulators by trapping ultracold atoms in the magnetic field of superconducting vortex lattice raises the need to develop methods to create vortex lattices of various symmetries. Here we propose layered systems where the vortex interaction is multiscale (in particular, the type-1.5 systems) as the systems where, in principle, various vortex lattice symmetries can be realized. The upper layer may, in particular, be used to tune localization of the field while lower layers and interlayer distances are used to control lattice symmetry. Different temperature dependencies of components in different layers can also be used to manipulate the vortex lattice by controlling the temperature. We support that proposal by simulation of point-particle objects with phenomenological two-body forces similar to long-range forces between straight and rigid vortex lines. Next we plan to investigate it in the layered Ginzburg-Landau model, which also include the effects of vortex bending and nonpairwise intervortex forces (which can be especially important in type-1.5 regimes [36]).

This work was supported by the National Science Foundation under the CAREER Award No. DMR-0955902, the Knut and Alice Wallenberg Foundation through a Royal Swedish Academy of Sciences Fellowship, and by the Swedish Research Council.

[1] I. Buluta and F. Nori, Science **326**, 108 (2009).
[2] J. I. Cirac and P. Zoller, Nat. Phys. **8**, 264 (2012).
[3] I. Bloch, J. Dalibard, and W. Zwerger, Rev. Mod. Phys. **80**, 885 (2008).
[4] I. Bloch, J. Dalibard, and S. Nascimbène, Nat. Phys. **8**, 267 (2012).
[5] D. M. Weld, P. Medley, H. Miyake, D. Hucul, D. E. Pritchard, and W. Ketterle, Phys. Rev. Lett. **103**, 245301 (2009).
[6] D. M. Weld, H. Miyake, P. Medley, D. E. Pritchard, and W. Ketterle, Phys. Rev. A **82**, 051603 (2010).
[7] C. J. M. Mathy, D. A. Huse, and R. G. Hulet, Phys. Rev. A **86**, 023606 (2012).
[8] O. Romero-Isart, C. Navau, A. Sanchez, P. Zoller, and J. I. Cirac, Phys. Rev. Lett. **111**, 145304 (2013).
[9] M. Gullans, T. G. Tiecke, D. E. Chang, J. Feist, J. D. Thompson, J. I. Cirac, P. Zoller, and M. D. Lukin, Phys. Rev. Lett. **109**, 235309 (2012).
[10] C. M. Aegerter, S. H. Lloyd, C. Ager, S. L. Lee, S. Romer, H. Keller, and E. M. Forgan, J. Phys.: Condens. Matter **10**, 7445 (1998).
[11] T. M. Riseman, P. G. Kealey, E. M. Forgan, A. P. Mackenzie, L. M. Galvin, A. W. Tyler, S. L. Lee, C. Ager, D. M. Paul, C. M. Aegerter, R. Cubitt, Z. Q. Mao, T. Akima, and Y. Maeno, Nature (London) **396**, 242 (1998).
[12] V. Moshchalkov, R. Woerdenweber, and W. Lang, *Nanoscience and Engineering in Superconductivity* (Springer, Berlin, 2010).
[13] M. Baert, V. V. Metlushko, R. Jonckheere, V. V. Moshchalkov, and Y. Bruynseraede, Phys. Rev. Lett. **74**, 3269 (1995).
[14] V. V. Moshchalkov, M. Baert, V. V. Metlushko, E. Rosseel, M. J. Van Bael, K. Temst, R. Jonckheere, and Y. Bruynseraede, Phys. Rev. B **54**, 7385 (1996).
[15] E. Rosseel, M. Van Bael, M. Baert, R. Jonckheere, V. V. Moshchalkov, and Y. Bruynseraede, Phys. Rev. B **53**, R2983(R) (1996).
[16] D. J. Morgan and J. B. Ketterson, Phys. Rev. Lett. **80**, 3614 (1998).
[17] A. N. Grigorenko, G. D. Howells, S. J. Bending, J. Bekaert, M. J. Van Bael, L. Van Look, V. V. Moshchalkov, Y. Bruynseraede, G. Borghs, I. I. Kaya, and R. A. Stradling, Phys. Rev. B **63**, 052504 (2001).
[18] A. N. Grigorenko, S. J. Bending, M. J. Van Bael, M. Lange, V. V. Moshchalkov, H. Fangohr, and P. A. J. de Groot, Phys. Rev. Lett. **90**, 237001 (2003).
[19] G. R. Berdiyorov, M. V. Milošević, and F. M. Peeters, Phys. Rev. B **74**, 174512 (2006).
[20] C. Reichhardt and C. J. O. Reichhardt, Phys. Rev. B **76**, 064523 (2007).
[21] R. Cao, L. Horng, T. C. Wu, J. C. Wu, and T. J. Yang, J. Phys.: Condens. Matter **21**, 075705 (2009).
[22] M. L. Latimer, G. R. Berdiyorov, Z. L. Xiao, W. K. Kwok, and F. M. Peeters, Phys. Rev. B **85**, 012505 (2012).
[23] Q. Chen, S. C. Bae, and S. Granick, Nature (London) **469**, 381 (2011).
[24] F. Romano and F. Sciortino, Nat. Mater. **10**, 171 (2011).
[25] X. Mao, Q. Chen, and S. Granick, Nat. Mater. **12**, 217 (2013).
[26] M. E. Cates, Nat. Mater. **12**, 179 (2013).
[27] E. Babaev and M. Speight, Phys. Rev. B **72**, 180502 (2005).
[28] M. Silaev and E. Babaev, Phys. Rev. B **84**, 094515 (2011).
[29] M. Silaev and E. Babaev, Phys. Rev. B **85**, 134514 (2012).
[30] J. Garaud, D. F. Agterberg, and E. Babaev, Phys. Rev. B **86**, 060513 (2012).
[31] V. Moshchalkov, M. Menghini, T. Nishio, Q. H. Chen, A. V. Silhanek, V. H. Dao, L. F. Chibotaru, N. D. Zhigadlo, and J. Karpinski, Phys. Rev. Lett. **102**, 117001 (2009).
[32] J. Gutierrez, B. Raes, A. V. Silhanek, L. J. Li, N. D. Zhigadlo, J. Karpinski, J. Tempere, and V. V. Moshchalkov, Phys. Rev. B **85**, 094511 (2012).
[33] V. H. Dao, L. F. Chibotaru, T. Nishio, and V. V. Moshchalkov, Phys. Rev. B **83**, 020503 (2011).
[34] C. W. Hicks, J. R. Kirtley, T. M. Lippman, N. C. Koshnick, M. E. Huber, Y. Maeno, W. M. Yuhasz, M. B. Maple, and K. A. Moler, Phys. Rev. B **81**, 214501 (2010).
[35] S. J. Ray, A. S. Gibbs, S. J. Bending, P. J. Curran, E. Babaev, C. Baines, A. P. Mackenzie, and S. L. Lee, Phys. Rev. B **89**, 094504 (2014).

[36] J. Carlström, E. Babaev, and M. Speight, Phys. Rev. B **83**, 174509 (2011).

[37] C. N. Varney, K. A. H. Sellin, Q.-Z. Wang, H. Fangohr, and E. Babaev, J. Phys.: Condens. Matter **25**, 415702 (2013).

[38] L. Komendová, M. V. Milošević, and F. M. Peeters, Phys. Rev. B **88**, 094515 (2013).

[39] H. Fangohr, A. R. Price, S. J. Cox, P. A. J. de Groot, G. J. Daniell, and K. S. Thomas, J. Comput. Phys. **162**, 372 (2000).

[40] H. Fangohr, S. J. Cox, and P. A. J. de Groot, Phys. Rev. B **64**, 064505 (2001).

[41] X. B. Xu, H. Fangohr, X. N. Xu, M. Gu, Z. H. Wang, S. M. Ji, S. Y. Ding, D. Q. Shi, and S. X. Dou, Phys. Rev. Lett. **101**, 147002 (2008).

[42] J. A. Drocco, C. J. O. Reichhardt, C. Reichhardt, and A. R. Bishop, J. Phys.: Condens. Matter **25**, 345703 (2013).

[43] G. Malescio and G. Pellicane, Phys. Rev. E **70**, 021202 (2004).

[44] M. A. Glaser, G. M. Grason, R. D. Kamien, A. KoÅ¡mrlj, C. D. Santangelo, and P. Ziherl, Europhys. Lett. **78**, 46004 (2007).

[45] J. Pearl, Appl. Phys. Lett. **5**, 65 (1964).

[46] The definition of the density is $\rho = N_v/L_xL_y$, where N_v is the number of vortices, and L_x and L_y are the box sizes of the simulation.

[47] The functional form of the potentials in Fig. 2 can be found in Appendix B of Ref. [37] [see Eq. (B5)]. The precise form of the potential is not particularly important as the two-dimensional lattices can be generated using a multitude of parameters, which we shall discuss elsewhere. The parameters for solid red line are $\alpha = 3.0$, $\beta = 1.5$, and $\xi = \lambda$ while for the dashed blue line they are $\alpha = 2.5$, $\beta = 0.5$, and $\xi = \lambda$. In both cases, we set $c_1 = 1$, $c_2 = 0.2$, $c_3 = 0.1$, $\lambda = 1$, and $\delta = 0.1$.

[48] Q. Meng, C. N. Varney, H. Fangohr, and E. Babaev (unpublished).